Metallicity in fullerides

Katalin Kamarás*[a] and Gyöngyi Klupp[a,b]

Received Xth XXXXXXXXXX 20XX, Accepted Xth XXXXXXXXX 20XX
First published on the web Xth XXXXXXXXXX 200X
DOI: 10.1039/b000000x

Metallic salts formed from fullerenes became popular because of their superconducting properties with a relatively high transition temperature, and were initially regarded as conventional metals and superconductors. Recently, owing to improved synthetic methods and a renewed interest in the study of their physical properties, many of them were found to exhibit exotic metallic and superconducting phases. In this paper, we summarize earlier results on unconventional metallic fulleride phases as well as the newly discovered extended fulleride superconductors. The proximity of the Mott transition, a typical solid-state effect, results in molecular crystals, where molecular spectroscopic methods prove very successful. We concentrate on infrared and optical spectroscopy which is very well suited to follow metallicity and phase transitions in this class of substances.

1 Introduction

Fullerenes were discovered more than 25 years ago, yet keep scientists fascinated ever since. Their simplicity and symmetry, coupled with their versatility enables them to be used as examples for many concepts in condensed matter physics, mainly related to electronic instabilities as electron correlations and superconductivity. As many new members of the family are emerging, due to sophisticated chemical preparation methods, they can be used to illustrate phenomena as correlated metallic and insulating behavior, the coexistence of superconductivity and electron correlations, and even non-conventional superconductivity. Here we review recent developments in this direction, concentrating on the metallic/non-metallic character in the normal state. The family of fullerenes is in itself a vast one, but we restrict the topic to its prime example, the C_{60} molecule and its molecular anions. (Therefore, throughout the paper, the term "fullerene" means strictly C_{60}.)

This paper is not meant to be a comprehensive review since such already do exist. Many of the instabilities have been discussed on the experimental side by Forró and Mihály[1] and theoretically by Capone et al.[2] The properties of fulleride salts of alkali and alkaline earth metals were presented in a unified framework by Iwasa and Takenobu.[3] Following the first discoveries of superconductivity in alkali fullerides, the general assumption was to regard them as simple metals, turning to Bardeen–Cooper–Schrieffer (BCS) superconductors below the transition temperature; in this sense, they were regarded "less interesting" than inorganic, for example cuprate, superconductors. This view was not shared by the whole community; even in the early days of fullerene research, other explanations were put forward, and as, thanks to innovative chemistry, more and more fulleride salts with sufficient purity have been synthesized, the signs are pointing towards novel mechanisms in both metallicity and superconductivity. We try to present an overview of these results and put them in perspective to show why we think fullerides, similarly to cuprates and organic conductors, are ready to take their place as model compounds for these mechanisms.

We adopt the point of view of the molecular spectroscopist, which has proven surprisingly useful when extended towards a more general condensed-matter approach.

2 Electronic structure

Metallic fulleride salts are composed of fulleride ions and cations, in most cases alkali or alkaline earth metal ions. To a first approximation, the latter act simply as electron donors to the fullerene molecules and the molecular ions can be regarded as the lattice sites providing the electrons that in turn form the band structure of the solid. The charge of these anions depends on the chemical composition, i.e. the charge donated by the cations per fullerene ball, the electronic properties are therefore largely determined by the composition.

The first Hückel calculation of the electronic structure of C_{60} by Haddon[6,7] is still a very good starting point to qualitatively understand the situation in fulleride salts. The sequence and population of the C_{60} molecular orbitals (Fig. 1) resembles that of atomic orbitals with increasing angular momentum quantum number L. However, to regard the fullerene molecule as a simple atomic core is grossly oversimplified; instead, it is truly a chemical entity capable of molecular distortions and chemical reactions. The icosahedral, instead of

[a] *Research Institute for Solid State Physics and Optics, Wigner Research Centre for Physics, Hungarian Academy of Sciences, Budapest, Hungary. Fax: 36 1 392 2219; Tel: 36 1 392 2222; E-mail: kamaras.katalin@wigner.mta.hu*
[b] *Department of Chemistry, Durham University, Durham, United Kingdom.*

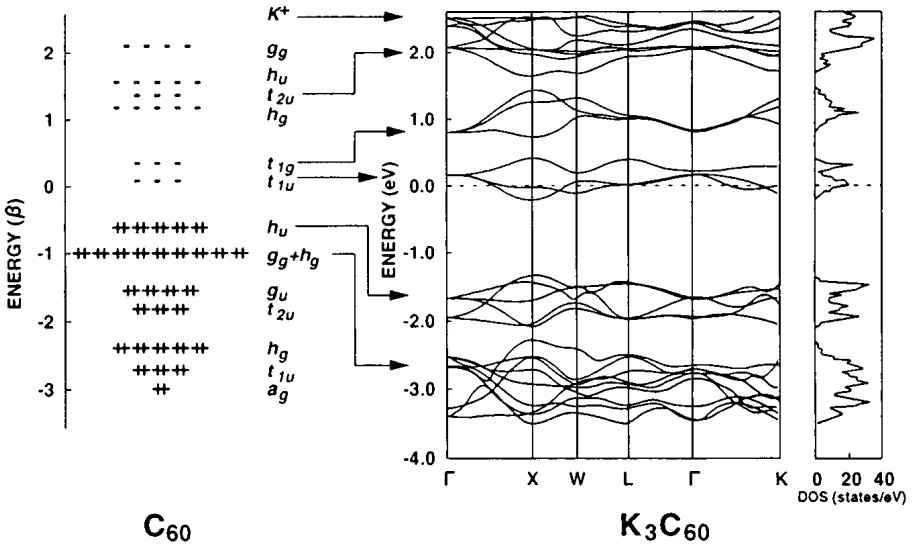

Fig. 1 The electronic structure of C_{60} and the band structure of A_3C_{60} after Hebard.[4] Reproduced from Ref. 5 (http://journals.aps.org/rmp/abstract/10.1103/RevModPhys.68.855). Copyright (1996) by the American Physical Society.

spherical, symmetry causes the removal of degeneracy in the levels analogous to L>3. The splitting relevant for the HOMO and LUMO levels is that of the L=5 level, containing 11 states, into h_u, t_{1u} and t_{1g} orbitals corresponding to the irreducible representations of the icosahedral point group I_h. Simple electron counting yields that the h_u level will be the HOMO containing ten electrons, and the LUMO and LUMO+1, respectively, will be able to accomodate six electrons each.

Based on the molecular results, Saito and Oshiyama[8] calculated the band structure of C_{60} and found it to be an insulator with a 1.5 eV direct bandgap. In this approximation, the HOMO band is based on the five h_u levels and the LUMO band on the three t_{1u} levels, with bandwidths around 0.5 eV. Adding electrons to a C_{60} molecule and building up a solid from it results in a very similar band structure where the conduction band is partially filled[9] (Fig. 1 illustrates the case for a solid built from trivalent fulleride ions). The band structure calculations based on the molecular orbitals give a very good starting point for the discussion of optical spectra. The direct transition between the HOMO and the LUMO is optically forbidden, but as soon as the LUMO becomes populated by electron doping, the LUMO $\rightarrow$ LUMO+1 transition will become allowed and show up around 1.1 eV. Higher-energy transitions in the optical spectra do not show significant changes compared to C_{60}.[10]

The t_1u LUMO band can accomodate up to six electrons and the results of the first experiments of doping C_{60} with alkali metals† showed that the highest concentration corresponds to A_6C_{60}. In the band picture of Fig. 1, when the LUMO-based band is partially filled, electrons have empty states to occupy in reciprocal space, meaning that they can propagate freely in real space (i.e. they cannot be assigned to any particular ionic core). An insulating state occurs if the band is either empty or completely filled; this is called a band insulator. Already at the time of discovery of conducting fullerides, it was noted[11,12] that the simple band picture yielded an unphysically short mean free path (shorter than the interfulleride distance). In such cases, instead of the band model, another one is used where the electrons are confined to the molecular ions, and move between them by "hopping". If the Coulomb repulsion between the electron and the nearest neighbor is too large, then it will prohibit hopping and the system will become an insulator despite the partial band filling in the band picture. Such a system is called a Mott insulator[13] and the change between metallic and insulating behavior a Mott transition.[14]

The concept of a Mott insulator[13] is indeed easy to grasp for a chemistry-trained mind. We start with a solid consisting of molecular ions, each keeping its electrons in its vicinity. If we move these ions closer to each other, the overlap between the electron clouds increases until a collective electron system is formed and the crystal turns into a metal. The intermolecular distance can be tuned by external pressure or by "chemical pressure" i.e. decreasing the size of the counterion and thereby the lattice constant. In condensed matter physics, the parameters used in this model are the on-site Coulomb repul-

† The formation of alkali fullerides is, strictly speaking, a chemical redox reaction between the metal and the fullerene, resulting in an ionic salt with a precise stoichiometric composition, and not quite analogous to doping of semiconductors; however, because of the widespread usage of the term in the literature of fullerenes, we will use it in this sense here.

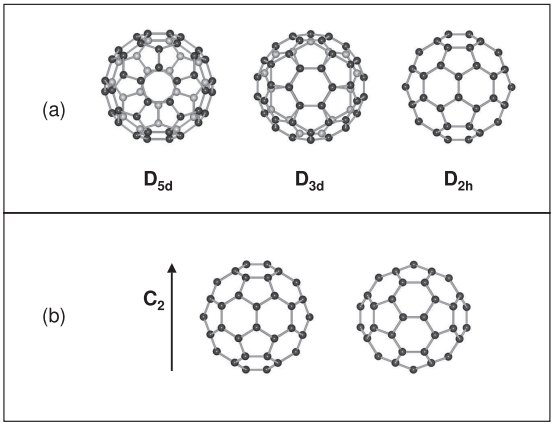

Fig. 2 (a) Possible symmetry-lowering distortions in fulleride ions: D_{5d}, D_{3d} and D_{2h}. The axis along which the distortion occurs is perpendicular to the plane of the paper through the center of the molecule. The atoms above the plane of the paper are black while those under it are grey. (b) The two "standard orientations" of fulleride ions in a crystal where the principal crystal axis coincides with one of the molecular C_2 axes. Static or dynamic average of these two orientations with D_{2h} symmetry results in overall tetragonal (D_{4h}) structure. Reproduced from Ref. 15 (http://journals.aps.org/prb/abstract/10.1103/PhysRevB.73.085415). Copyright (2006) by the American Physical Society.

sion U, the energy required to add an electron to the ion, and the bandwidth W, which is related to the intermolecular overlap. The Mott transition occurs if the system reaches a critical U/W value, the "Mott limit". U is in first approximation the difference between the ionization potential and the electron affinity of the ion (the cost of converting a pair from two identically charged ions to one where an excess charge was taken from one of the ions and put onto the other). U is therefore a molecular property, and W is influenced by the intermolecular distance and symmetry which determine the overlap.

An additional complication arises because here the "cores" are not atoms, but molecules. The icosahedral cage, consisting of sixty atoms forming one of the most symmetric shapes found in nature, is inherently sensitive to symmetry-lowering effects. (These play a much less important role in other organic conductors and superconductors, where the complicated organic molecules form crystals with very low symmetry.) The primary effect is the crystal field, determined by the arrangement of the counterions. If the symmetry of the crystal is lower than cubic, the degeneracy of the t_{1u} orbitals is lifted and the formerly partial occupation can become full. The symmetry lowering and the resultant splitting of the triply degenerate t_{1u} levels is determined by the largest common subgroup of the icosahedral group and the space group of the crystal. Possible axes of molecular distortion into the three subgroups D_{5d}, D_{3d} and D_{2h} are indicated in Fig. 2(a). The distortions consist of elongation or compression along these axes. Figure 3 illustrates the splitting for possible high-symmetry crystal structures. It is worth noting that there occurs a threefold splitting in tetragonal crystals, a consequence of the lack of a fourfold axis in icosahedral symmetry. (The average symmetry in tetragonal crystals is the result of orientational disorder of D_{2h}-distorted fulleride anions in the tetragonal lattice formed by the cations, as shown in Fig.2(b).[16]) The crystal structure is mostly determined by size effects:[12] for A = K and Rb, A_3C_{60} salts are face-centered cubic, A_4C_{60} body-centered tetragonal and A_6C_{60} body-centered cubic. In salts with organic cations, the symmetry can be even lower but the splitting will stay threefold as the degeneracy is completely lost already in the orthorhombic environment.

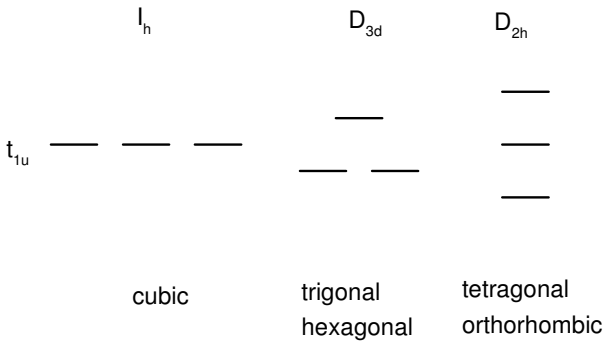

Fig. 3 Symmetry lowering and crystal-field splitting of t_{1u} levels in various crystallographic systems. In the case of twofold splitting, the order of levels is arbitrary. D_{5d} does not occur in crystals since it is not a crystallographic point group.

Considering the abundant orbital degeneracy, the Jahn–Teller distortion is obviously another possibility for symmetry reduction. As the prerequisite for Jahn–Teller coupling is the partial filling of degenerate orbitals, it is easy to comprehend that any fulleride anion with charges different from 0 or 6 should be a candidate. Details of the Jahn-Teller effect in fullerides have been extensively discussed in reference works.[17,18] Nevertheless, we recall the main results here to emphasize the difference from inorganic systems.[19]

In a coordination compound with a central metal ion, the Jahn–Teller distortion means that following the splitting of the degenerate orbitals of the central ion, the ligands rearrange in a different geometry of lower symmetry. If the system is a crystal, this change corresponds to a structural phase transition, since the rearrangement in one unit cell results in the rearrangement of all others to obey translational symmetry. A C_{60}^{n-} molecular ion, on the other hand, can undergo a Jahn–Teller

distortion by reshaping the molecule itself, without perturbing the environment. Speaking in terms of electron–phonon coupling, the vibrations coupled to the electronic system are intramolecular in the case of fullerenes, unlike the inorganic compounds, where the relevant vibrations happen between the central atom and the ligands. A striking example for this difference is that fulleride anions can show Jahn–Teller distortions in the gas phase[20] or in solution.[21]

In a crystal the Jahn–Teller distortion competes with the crystal field of the surrounding cations. While the crystal field induces a static distortion which can be detected by diffraction methods,[22,23] the Jahn–Teller effect can induce several almost equivalent distortions along symmetry-related axes in different directions: six for D_{5d} symmetry, ten for D_{3d} symmetry and twelve for D_{2h} symmetry. (When the crystal field is weak, translation symmetry is not obeyed any longer by the fulleride ions and therefore D_{5d} is also allowed.) If the barrier between these distortions is small, the system can move between them via pseudorotation[17] if it acquires sufficient thermal energy.

The Jahn–Teller effect can only happen if the carriers are localized on the anions, i.e. they are below the Mott limit for conduction. On the other hand, the Jahn–Teller effect promotes the Mott transition by lowering the energy of the anion in the distorted state. Using the concept of such "Mott–Jahn–Teller nonmagnetic insulators", the electronic and magnetic properties of A_4C_{60} salts were successfully modeled.[24,25] Jahn–Teller distortions, like other types of symmetry lowering, can be very sensitively detected by vibrational spectroscopy.[26]

3 Optical and infrared spectroscopy in fulleride research

3.1 Electronic transitions

Conclusions regarding metallicity can be reliably drawn from the low-frequency optical spectra (in the far- and midinfrared). The frequency-dependent (optical) conductivity is a function which reflects charge dynamics in the solid and can be determined from measured optical quantities as transmission or reflectance, provided the measurement extends over a wide enough frequency range.[27] For opaque samples as the metallic fullerides, the measurement of reflectance, evaluated by Kramers–Kronig transformation,[28,29] yields the optical conductivity. Extrapolating the frequency-dependent conductivity to zero gives the dc conductivity and can be compared to transport measurements. Figure 4 shows the reflectivity curves of C_{60} and the metallic fulleride K_3C_{60}. Insulators as C_{60} exhibit a flat low reflectivity up to the first electronic transition (with a slight structure in the infrared due to vibrational transitions, see below), while metallic electrons cause high reflectivity in the low-frequency region (Drude absorption), followed by an abrupt decrease (the plasma edge). The optical conductivity calculated from reflectance spectra is the function directly comparable to band structure calculations.

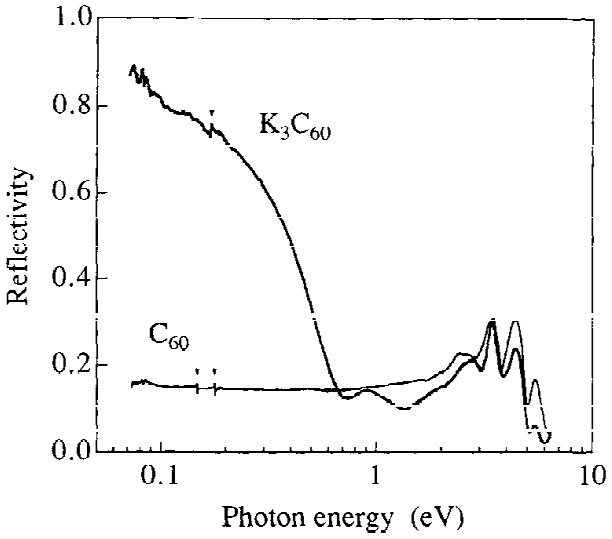

Fig. 4 Room-temperature reflectance spectra of C_{60} and K_3C_{60} fulleride. Note the logarithmic energy scale, 1 eV corresponds to 8065 cm^{-1}. The frequency extends from the far infrared through the ultraviolet. Reproduced from Ref. 10 (http://journals.aps.org/prl/abstract/10.1103/PhysRevLett.69.2284). Copyright (1992) by the American Physical Society.

3.2 Vibrational spectroscopy and vibronic coupling

The C_{60} molecule has 174 vibrational degrees of freedom, but due to the high symmetry, only 4 of those are infrared active.[6,30] These infrared-active modes in unperturbed C_{60} are of T_{1u} symmetry (sometimes denoted by F_{1u}), same as the LUMO. Thus the splitting of the vibrational modes, detected by infrared spectroscopy, mirrors the splitting of the LUMO in the anions (Fig. 3). Lowering of molecular symmetry will cause splitting of allowed modes and activation of silent modes in the infrared spectrum and is therefore a sensitive indicator of molecular distortions.

Contrary to conventional metals, vibrational transitions can be present even in the metallic state of fullerides and the details of these vibrational bands often convey important information. These weak features cannot be very well measured by reflectivity, instead the usual chemical infrared method of KBr pellets is used. Figure 5 shows the infrared transmission of a metallic and an insulating fulleride salt compared to C_{60}. These spectra can be recorded with very high resolution (typically well below 1 cm^{-1}) and fine details of the vibrational structure are detected this way. Because of the high reflectivity of most fullerides, especially towards the far in-

frared, the optical density derived from the transmission (-log T) does not correspond to the absorption with enough accuracy to compare it to results from theory.[31] (This is the reason why we present our results as transmission curves in most cases.) The most important information is the frequency of the vibrational bands, the lineshape, and their change with external parameters like temperature or pressure. For the same pellet under varying conditions, a semiquantitative scaling can also be done. In practical terms, the KBr method has the advantage of preserving the composition of the samples, often arrived at by complicated synthetic pathways, and can be used under exclusion of air, as most fulleride salts are air-sensitive. KBr is transparent above 400 cm^{-1} (0.05 eV) up to the ultraviolet, therefore infrared and near-infrared spectra of the vibronic transitions and low-frequency interband transitions can be studied.

The samples have to be handled under strict exclusion of air and water, preferably in an inert gas dry box. We press our pellets under argon atmosphere and perform initial screening with a low-resolution FTIR spectrometer in an argon dry box, then fill the sample into a cryostat and do all measurements under dynamical vacuum. Reflectivity is measured in the same way, except that in this case, neat pellets[28] or films with high surface quality[10] are used. It is a good idea to coat the pellets with a metal layer after the measurement and use this spectrum as reference instead of a flat metal mirror, in order to correct for surface imperfections.[28]

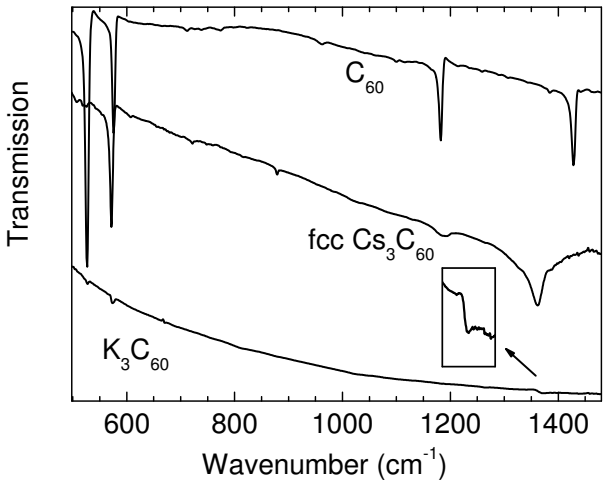

Fig. 5 Infrared transmission spectra of C_{60}, a metallic (K_3C_{60}), and an insulating (expanded Cs_3C_{60}) fulleride.[32,33] The inset shows the Fano lineshape of the $T_{1u}(4)$ mode in K_3C_{60}.

Although the relationships connecting bulk reflectivity and KBr pellet transmission are too complicated for an exact description (mainly due to multiple scattering in the pellets), there are a few features in the transmission spectra indicating metallic behavior. One is the high background absorption

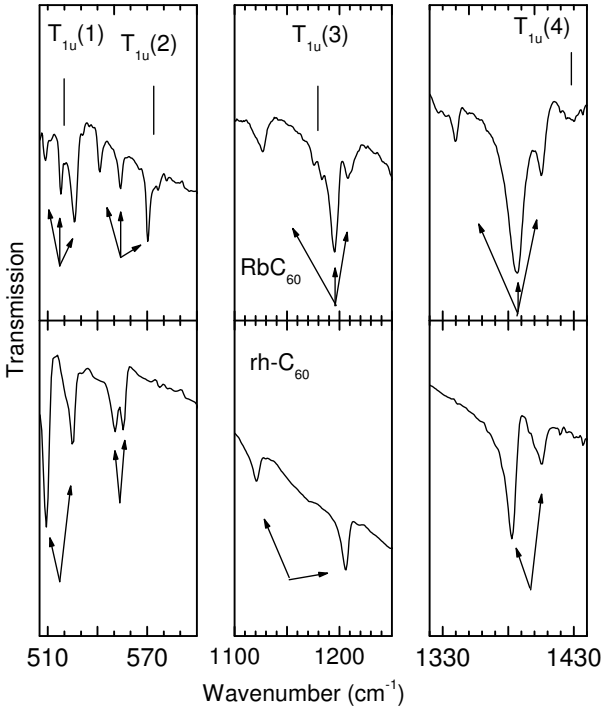

Fig. 6 Splitting of the T_{1u} modes in the infrared spectra of C_{60}-based polymers: RbC_{60} (D_{2h}) and rh-C_{60} (D_{3d}).Reproduced from Ref. 36 (http://journals.aps.org/prb/abstract/10.1103/PhysRevB.55.10999). Copyright (1997) by the American Physical Society.

in the infrared, corresponding to the high reflectivity, the other is the lineshape of the vibrational bands. Figure 5 shows the transmission of C_{60} and two of its salts, an insulator and a metal. Metallic K_3C_{60} shows a strong and almost featureless absorption compared to C_{60} and the insulator Cs_3C_{60}. In addition, the lineshape of the highest frequency vibrational mode changes as shown in the inset of Fig. 5. The mechanism behind the lineshape is the Fano effect,[34] the interaction of a localized excitation with a continuum. Here, the continuum is formed by the delocalized electrons and the localized mode is the molecular vibration. The mechanism is further explained for infrared spectra of organic conductors by Tanner et al.[35]

The effect of symmetry reduction on the vibrational modes can be studied on fullerene-based polymers, where the structural changes are considerable because of the forming of intermolecular bonds.[36–39] Figure 6 illustrates the splitting of the triply degenerate T_{1u} modes in two C_{60}-based polymers, linear RbC_{60} with D_{2h} symmetry and two-dimensional rhombohedral $(C_{60})_n$ with D_{3d} symmetry. We observe threefold splitting for the former and twofold splitting for the latter of all modes, in accordance with group theory predictions.[36‡] The

‡ Ref. 36(a) should be read together with its erratum,[36] because of an error in

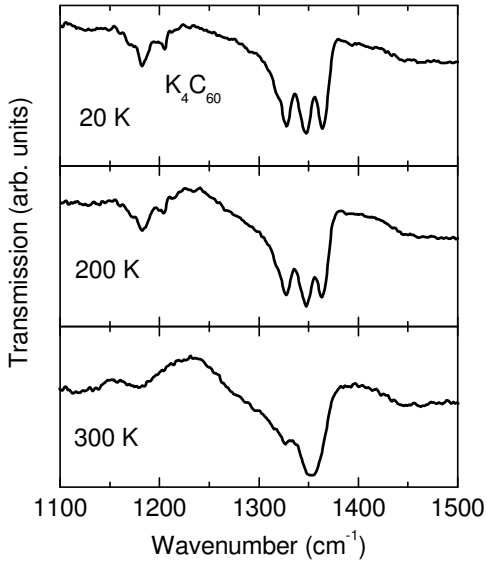

Fig. 7 Splitting of the $T_{1u}(4)$ vibrational mode in the infrared spectra of K_4C_{60} at different temperatures. Reproduced from Ref. 42 (http://journals.aps.org/prb/abstract/10.1103/PhysRevB.65.052103). Copyright (2002) by the American Physical Society.

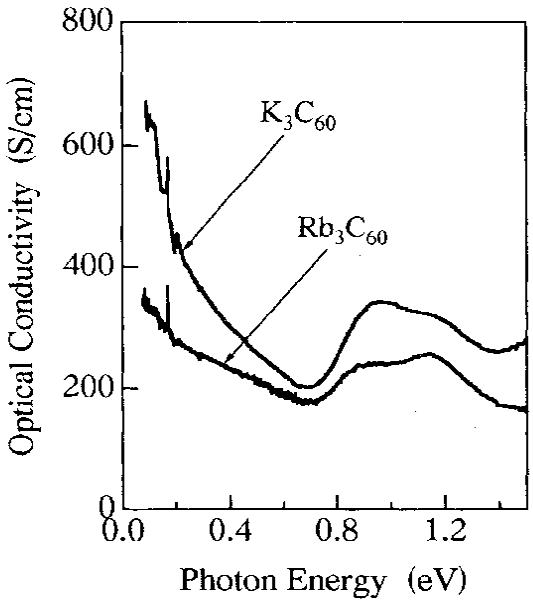

Fig. 8 Infrared optical conductivity of K_3C_{60} and Rb_3C_{60}. Reproduced from Ref. 29 (http://journals.aps.org/prb/abstract/10.1103/PhysRevB.51.3678). Copyright (1995) by the American Physical Society.

frequency of the $T_{1u}(4)$ mode, at 1429 cm^{-1} in C_{60}, strongly depends on the charge[40] and the bonding pattern[41] and is used as a general indicator for these characteristics.

Similar, but more complicated effects are expected for the Jahn–Teller distortion in A_4C_{60}, where a competition exists between the Jahn–Teller dynamics and the tetragonal crystal field. The splitting of the $T_{1u}(3)$ and $T_{1u}(4)$ modes changes with temperature[42] (Fig. 7), while the crystal structure is preserved between 4 K and 300 K and thus there is no change in the symmetry of the crystal field.[15] At low temperature the anion assumes D_{2h} symmetry, compliant with the tetragonal crystal field (Fig. 3), resulting in threefold splitting of the modes. At room temperature, a twofold splitting is apparent, which corresponds to the inherent Jahn–Teller distortion of a C_{60}^{4-} ion.[43] This Jahn–Teller distortion is dynamic, so that the average structure will remain tetragonal but the deformation is observed on the time scale of the infrared measurement. The pseudorotation in the dynamic Jahn–Teller state is made possible by the lattice expansion, and consequently, the transition temperature scales with the size of the cation in the A_4C_{60} (A=K,Rb,Cs) series.[15] Unlike polymers, where the bond lengths change considerably, in this case diffraction studies give an upper limit of 0.04 Å for the distortion,[16] indicating the sensitivity of spectroscopy to detect molecular deformation.

the original correlation table.

4 Metallic fullerides

4.1 Trivalent salts of K and Rb

The earliest measurements of IR transmission[44] or reflectance[40] were conducted on thin films starting from C_{60} while in-situ doping by alkali metals and monitoring the resistivity. As these measurements had to be conducted in specially constructed cells, no other type of characterization was possible, making the assignment of stoichiometry difficult. Nevertheless, these results showed that while the resistivity decreased towards the A_3C_{60} composition and increased subsequently up to A_6C_{60}, the overall transmission also showed an analogous pattern. Resistivity and optical data on A_3C_{60} (where A is both K and Rb) indicated metallic character of this composition, which was further proven by reflectivity data on single-phase powders pressed into pellets.[28]

Concerning the optical properties and metallicity, the papers by Iwasa et al. on A_3C_{60}[10,29] and A_4C_{60}[29] are of fundamental importance. Figure 4 shows the wide-range reflectivity of C_{60} and K_3C_{60} at room temperature. The principal difference is the low-frequency absorption by free carriers, but the vibrational features in both samples are also evident. The optical conductivity of K_3C_{60} and Rb_3C_{60} is compared in Fig. 8. The higher intensity of the free-carrier absorption in K_3C_{60} indicates that it is a better metal, in accordance with its smaller lattice constant and consequently higher overlap.

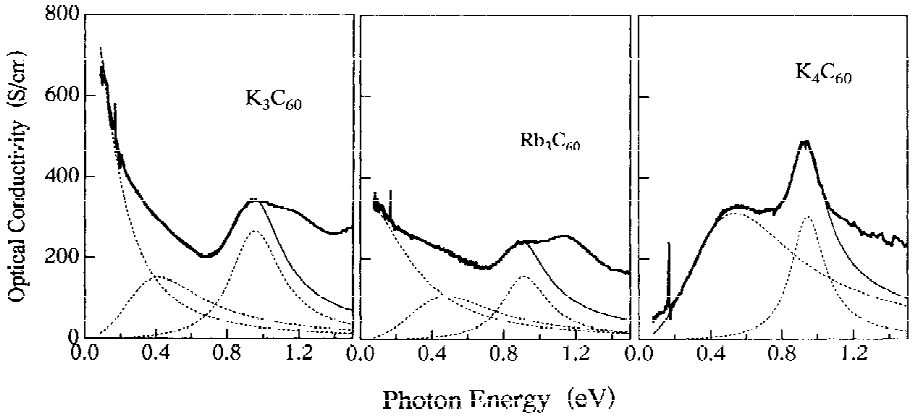

Fig. 9 Drude-Lorentz fits to the optical conductivity of K_3C_{60}, Rb_3C_{60} and K_4C_{60}. Reproduced from Ref. 29 (http://journals.aps.org/prb/abstract/10.1103/PhysRevB.51.3678). Copyright (1997) by the American Physical Society.

Palstra et al.,[45] based on the mean free path of the order of the interfullerene distance,[14] gave an estimate of 500–700 $(\Omega\text{cm})^{-1}$ for the limiting conductivity value for the Mott transition in A_3C_{60}. Their experiments show that Rb_3C_{60} reaches this limit around room temperature, while K_3C_{60} stays in the metallic regime up to much higher temperatures. There is no saturation in the increase of the resistivity in either case,[12] another sign attributed to electron correlations. A low mean free path and absence of resistivity saturation is called "bad metal" behavior and is an intriguing and not fully understood direction of condensed matter and materials physics.

The dc conductivity derived from the low-frequency extrapolation of the curves in Fig. 8 agrees remarkably well with the resistivity measurements mentioned above. Comparing the "Mott limit" estimate of Ref. 45 with the room-temperature optical conductivity data shown in Fig. 8 (Ref. 29), the extrapolated zero-frequency value for Rb_3C_{60} (355 $(\Omega\text{cm})^{-1}$) is around this limit, while that of K_3C_{60} (870 $(\Omega\text{cm})^{-1}$) is on the metallic side.

Analysis of the optical conductivity revealed that it cannot be described by a simple Drude model, instead, two Lorentz oscillators representing localized excitations had to be added (Fig. 9). Figure 9 compares the deconvolution of the optical conductivity of K_3C_{60}, Rb_3C_{60} and K_4C_{60}.[29] The appearance of such a "midinfrared absorption" has been noted before in other "bad metal" families: cuprates[47] and organic conductors.[48] Here the low-frequency absorption bands can be assigned to intermolecular electron transfer, in other words hopping of localized electrons. In insulating K_4C_{60} and its analogues such excitations were observed by electron energy loss spectroscopy[49] and IR transmission.[15] It seems that in the conducting phases these localized excitations persist beside the free-carrier absorption.

In Fig. 10 we present transmission data in KBr pellets on trivalent alkali fullerides. The background absorption in Rb_3C_{60} increases with decreasing temperature, following the increase in the conductivity. The lineshape around the $T_{1u}(4)$ vibrational mode depends on the cation: K_3C_{60} still shows the metallic Fano lineshape at 300 K, while in Rb_3C_{60} the low-temperature Fano lineshape starts to evolve towards a Lorentzian around room temperature. The transition from Lorentz to Fano corresponds to the Mott limit.

4.2 Low-dimensional polymers

Due to its unsaturated bonds, the C_{60} molecule is prone to polymerization reactions and the subsequent formation of low-dimensional structures. The first intermolecular reaction observed was [2+2] cycloaddition. According to the Woodward-Hoffmann rules, this reaction is forbidden between two ground-state neutral molecules, but becomes allowed if one of the reactants is in a photoexcited triplet state or an anion where the t_{1u} level is populated (Fig 11). In the latter case, the resulting polymer has an unpaired electron in its π^* level, and because of the shortened bond length, can propagate along the polymerization axis (Fig. 12.

The phase diagram of AC_{60} (A=K,Rb,Cs) is a very rich and varied one, depending not only on temperature but also on thermal history.[1,51] From structural, optical, thermal, conductivity, ESR and NMR studies and theoretical calculations, a consistent picture emerged. Three types of molecular structure appear in the phase diagram: monomeric anions, singly-bonded dimers and [2+2] cycloadduct polymers. The polymer phase forms during initial synthesis from the alkali metal and the fullerene powder; on heating, it depolymerizes into an fcc monomeric structure, consisting of separated C_{60}^- ions; fast cooling of this phase results in dimers at low temperature. Slow warming of this dimer phase yields first a monomeric phase around room temperature, followed by repolymeriza-

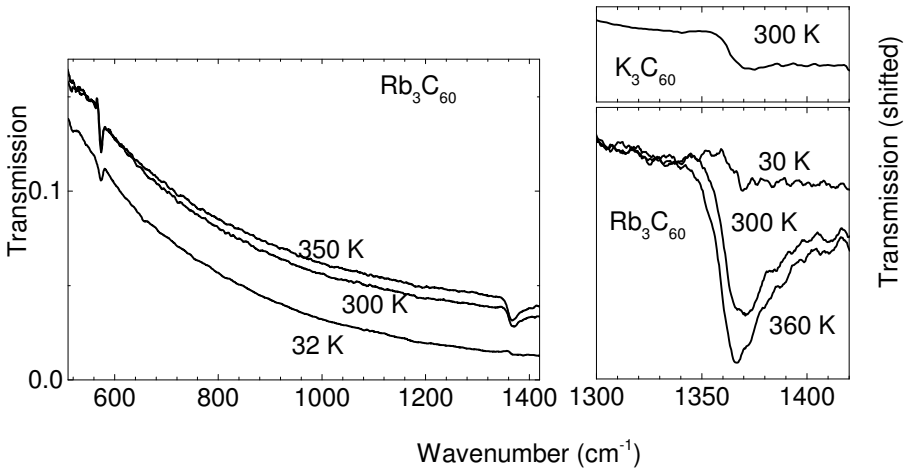

Fig. 10 Infrared transmission spectra of K_3C_{60} at room temperature and Rb_3C_{60} at various temperatures[46] in the $T_1u(4)$ vibration region. In Rb_3C_{60} the lineshape evolves from a Fano lineshape to a Lorentzian with increasing temperature; K_3C_{60}, which is a better metal, still shows Fano behavior at room temperature.

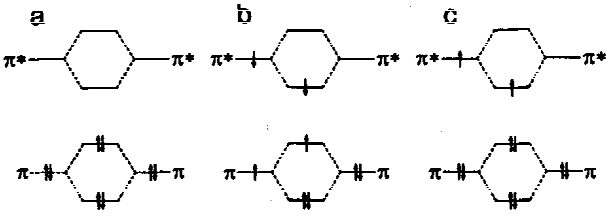

Fig. 11 Energy diagram of frontier orbital interactions in [2+2] cycloaddition reactions. The reaction between two ground state molecules is forbidden according to Woodward-Hoffmann rules (a); reactions between a photoexcited and a ground state molecule (b) and between anions (c) are allowed.[50] Copyright (1994) with permission from Elsevier.

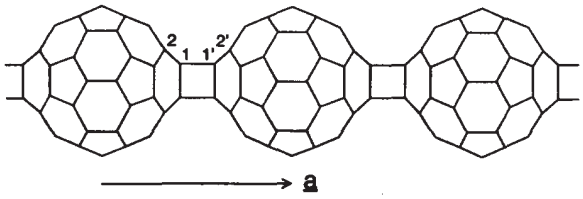

Fig. 12 Polymerization pattern in AC_{60}.[50] Copyright (1994) with permission from Elsevier.

tion to the [2+2] cycloadduct. These reactions were followed by calorimetry and spectroscopy.[52] Infrared spectroscopy is especially suited for identifying various phases in this case, because of the changes in molecular symmetry. The splitting of the T_{1u} modes (Fig. 13) is in agreement with D_{2h} symmetry in the polymer,[53] and C_s in the dimer (in the latter, one has to take into account the full C_{2h} symmetry of the dimer unit and work out the correlation tables accordingly[54]). Because the ions are rotating in the monomer phase, the symmetry there can be taken as I_h.

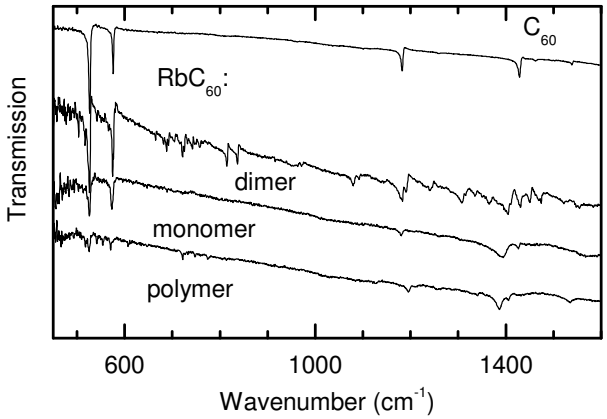

Fig. 13 Infrared transmission spectra of C_{60} and various phases of RbC_{60} in KBr pellet.[54] Except for C_{60}, the background was not shifted along the vertical axis.

In Fig. 13, one KBr pellet is followed by infrared spectroscopy through a heat treatment sequence: starting from the polymer, the sample was heated to 425 K where depolymerization to the monomer phase occurred, then quenched to 77

K to produce the dimer phase. During the procedure, both the vibrational structure and the background change. The kinetics of the phase transitions was monitored in a more detailed way by Martin et al.[55] on films, using the background transmission in the featureless part of the spectrum, at 900 cm^{-1}. Both measurements confirm that the polymer is the most conducting phase, followed by the monomer, while the dimer phase can be regarded as an insulator. With increasing metallic background, the vibrational peaks become less prominent, but there are still distinct Lorentzian lineshapes in the monomer and polymer phase. The polymer phase is considered a correlated one-dimensional metal in this temperature range, based on ESR and microwave conductivity measurements, turning into a three-dimensional correlated metallic system with a lower conductivity upon depolymerization.[56,57]

Over the years, several other polymeric fullerene derivatives have been prepared, many of them showing metallic character. According to quantum chemical calculations[58] the preferred bonding pattern changes from [2+2] cycloaddition at low anionic charge (0 or 1) to single intermolecular bonds at higher charge (3 or 4). Experimental facts prove these results: Na_4C_{60} has a two-dimensional structure where the tetravalent anions are connected by single bonds.[59] The spin susceptibility measured by ESR indicated a strongly correlated metal, similar to RbC_{60} or CsC_{60}. Na_2RbC_{60} has a polymorph with a similar bonding pattern but a structure consisting of one-dimensional chains.[60,61] ESR measurements found a Pauli-like susceptibility indicating a good metal.[1] As in these structures the sp^3 carbons prevent the formation of an aromatic system and thereby a full delocalization of electrons,[58] it seems that electron transport can be described as of the Mott-Hubbard type rather than a band-like behavior.

4.3 Small cations: multiple site occupation and diffusion

In fulleride salts with cations larger than Na, the size of the trigonal aperture connecting the interstitial sites prevents the motion of the cations between these sites. For Na and smaller ions, however, interesting phenomena occur because clusters of more than one atom (not necessarily all ionized) fit into the interstitial sites, and these cations can be mobile.

The salt with the composition Na_2C_{60} did not fit into the series of the other alkali metal fullerides: by electron-hole symmetry it should behave as a Mott–Jahn–Teller insulator analogous to the A_4C_{60} salts, yet early results showed metallic character at low temperature[62,63] and an infrared spectrum typical of multiphase material at room temperature. As it turns out, homogeneous single-phase Na_2C_{60} only exists above 460 K, below this temperature segregated nanodomains of C_{60} and metallic Na_3C_{60} are formed.[64] The separation disappears on heating by jump diffusion of the Na^+ ions. In the high-temperature phase, the infrared spectrum corresponds exactly

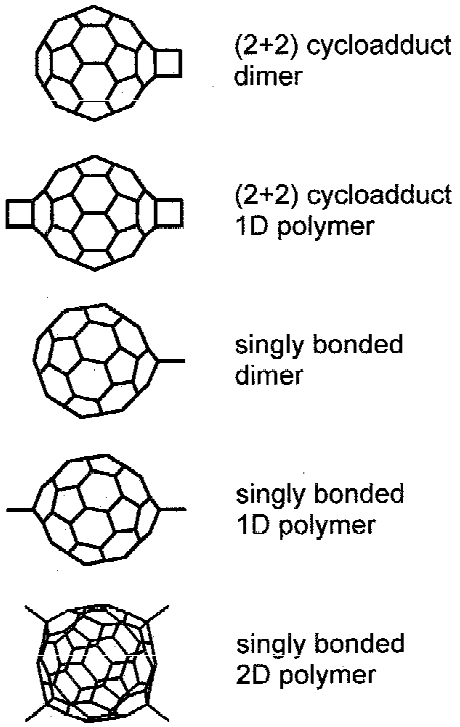

Fig. 14 Possible bonding motifs of C_{60}-based polymers.[58] Copyright (1998) with permission from Elsevier.

to a Jahn–Teller distorted C_{60}^{2-} ion, with D_{3d}/D_{5d} symmetry.

A special case of polymers is Li_4C_{60}.[65,66] This structure combines the [2+2] cycloaddition and single intermolecular bonding and results in a 2-dimensional network. Octahedral voids in the crystal can accomodate up to four lithium ions and the diffusion barrier is very low (about 0.2 eV). These conditions make ionic conduction possible and Li_4C_{60} indeed is proven to be a superionic conductor.[67] Diffusion of lithium ions was also observed in thin films of Li_4C_{60} by photoemission.[68] It is interesting that for both the bulk and thin film samples, experimental evidence points to partial charge transfer from Li to C_{60}: in the films, photoemission of C_{60},[68] and in the bulk, the shift of the Raman $A_g(2)$ mode.[66] Both estimates give around 2-2.5 electrons per C_{60}. As the mobility of the lithium ions excludes possible coordination bonds between Li and the fullerene cage, it is more probable that the partial charge transfer is related to Li ion mobility and the formation of transient clusters with less than one charge per ion. The depolymerization of Li_4C_{60} occurs above 600 K where the charge transfer reverts to 4 (proven by Raman spectra) and metallicity is restored.[69] The coexistence of tetravalent anions and metallicity indicates that Mott localization is absent in this material, i.e. the bandwidth is larger than the Jahn–Teller splitting. Recently, ionic conductivity has been found in Mg_2C_{60}, a polymer isostructural to Li_4C_{60}.[70]

4.4 Anions with charge n>3 and non-ionic bonding

Intercalation of C_{60} with alkaline earth ions adds electrons to the t_{1g} orbitals. The properties of these materials have been summarized by Iwasa and Takenobu.[3] Many of them are metals, despite the low-symmetry crystal structure, with (Ba_4C_{60})[71] or without (Ba_6C_{60}, Sr_6C_{60})[72] a superconducting transition. Metallicity was attributed in these materials to hybridization between 5d orbitals of Ba and t_{1g} orbitals of C_{60}.

A special member of this family is Mg_5C_{60}, a two-dimensional conducting polymer.[73] It is metallic at high temperature and turns insulating on cooling, the transition being attributed to Anderson localization on impurities. The infrared spectrum of this polymer is very different from the ones discussed so far; the highest-frequency infrared band is much higher than the $T_{1u}(4)$ mode of C_{60} and it coincides with a Raman mode (Fig. 15). The Raman frequency is also upshifted from the C_{60} $A_g(2)$ value of 1468 cm^{-1}, unlike Ca and Ba salts which show a downshift proportional to the nominal charge of the fulleride ion.[3]

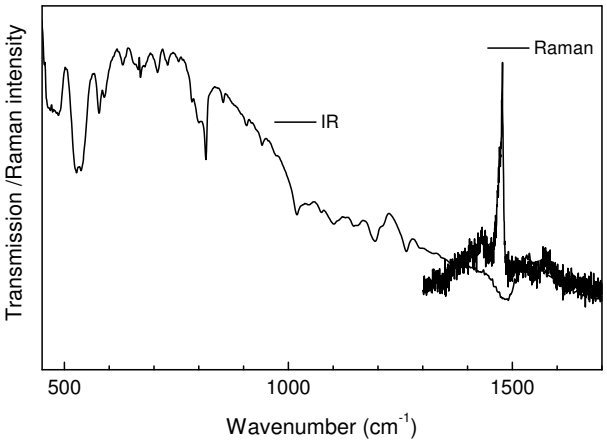

Fig. 15 Infrared and Raman spectra of Mg_5C_{60}. Reproduced from Ref. 73 (http://journals.aps.org/prb/abstract/10.1103/PhysRevB.77.155431). Copyright (2008) by the American Physical Society.

The most probable explanation for the newly appearing mode is that it is a Raman-active vibration activated by symmetry reduction due to covalent bonding to the Mg ion. A similar effect was reported for C_{60} monolayers adsorbed on metal[74] and semiconductor surfaces[75] and attributed to the $A_g(2)$ mode rendered infrared active by symmetry reduction and amplified by the "vibrational phase relaxation" mechanism.[76] This mechanism requires an electronic continuum and low-frequency vibrational and translational modes. The low-frequency modes are present in the polymer as the vibrations involving intermolecular bonds, and the whole effect is thus indirect proof for the presence of free electrons. The blueshift of both the infrared and Raman band is further indication for strong hybridization effects.

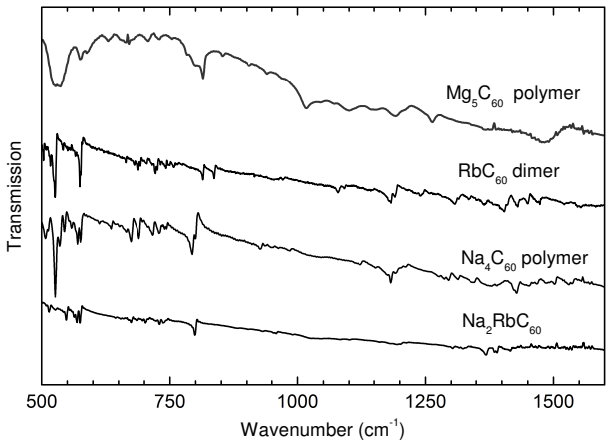

Fig. 16 Comparison of the infrared spectra of various singly bonded fulleride oligo- and polymers. Reproduced from Ref. 73 (http://journals.aps.org/prb/abstract/10.1103/PhysRevB.77.155431). Copyright (2008) by the American Physical Society.

Infrared spectroscopy can also help in identifying bonding patterns in polymers (Fig. 16). The intermolecular single bond has a specific infrared signature around 815 cm^{-1}, present in all polymers containing such bonds, including single-bonded dimers. From the infrared spectra the presence of single bonds in Mg_5C_{60} could be established.

The lineshape of the vibrational bands in metallic polymers (Fig. 16) is not Fano-like, despite the delocalized character of the electrons inferred mostly from magnetic susceptibility. This behavior is probably analogous to the "bad metal" phase which develops above room temperature in Rb_3C_{60} (Fig. 10). We have observed similar changes before, in organic conductors when changing the mean free path by the introduction of defects.[77] In a bad metal state, both local vibrational and electronic transitions (Fig. 9) seem to coexist with the free-carrier response.

5 Suppression of metallicity by correlations

Superconductivity of fullerides is certainly the principal driving force behind the study of their metallic properties. We do not intend to go into the details of the superconducting state, as several excellent reviews on this subject exist.[2,78] The search for new metals was driven by the possibility of increasing the superconducting transition temperature T_c. The T_c of early fcc alkali fullerides showed a linear dependence on the interfulleride distance, as was expected from the BCS theory. It was believed that the best way to increase T_c would be to prepare new crystals with increased lattice constant. If we take correlations into account, however, then at some interfullerene

distance Mott localization would occur and both metallicity and superconductivity disappear.

Dahlke et al.[79] prepared a series of trivalent Cs-containing "extended" fulleride salts, and found T_c to decrease systematically with distance. This "dome-like" dependence is typical of other families of superconductors (cuprates, heavy fermions, organic salts) where correlations play a significant role. More recently, the bottom of the dome was reached with insulating materials $(NH_3)K_3C_{60}$ and two polymorphs of Cs_3C_{60}, which however turn superconducting at slight pressure. All these observations point to these systems being on the verge of a Mott transition with the interfulleride distance controlling the parameter U/W. The exact mechanism behind the metal-insulator transition, however, is thought different in the two cases.

5.1 Loss of metallicity by reduction of symmetry

One of the first attempts to increase the lattice constant was the insertion of ammonia into the octahedral voids of K_3C_{60} (Ref. 80). The crystal structure of the resulting $(NH_3)K_3C_{60}$ is orthorhombic with a very slight distortion compared to fcc K_3C_{60}, but it is an insulator. Localization of the electrons on the C_{60}^{3-} sites is further proven by antiferromagnetic order developing at 40 K.[3] As other ammonia-containing fullerides with similar interfulleride distances are conducting,[81] the source of the difference was suggested to be the symmetry lowering. The site symmetry of C_{60}^{3-} is C_i,[82] causing a threefold orbital splitting shown in Fig. 3, and the observed S=1/2 spin state corresponds to double occupancy of the lowest lying orbital and single occupancy of the next. Dynamical mean-field theory calculations[83] indeed showed that the system is so close to a Mott transition that the width of the split electronic bands is smaller than their energy difference. Pressure can drive the system across the Mott limit, resulting in a superconductor with T_c=28 K at 14 kbar. However, even the normal state is not without special features: the antiferromagnetic ordering below 40 K is preceded by a structural transition to an orientationally ordered phase, where the rotation of both ammonia and fulleride molecules is stopped and neighboring fulleride anions are fixed in two distinct orientations related by a 90° rotation around the *c* axis (Fig.2(b)), in a regular pattern. This pattern is called "ferrorotative" or "antiferrorotative", depending on the relative position of the two orientations. Rotational and magnetic order seem to be related and analogous to multiferroic behavior in inorganic systems.

5.2 Superconductors with Mott-Jahn-Teller insulating normal state

The material where fulleride anions are enclosed in the most symmetric environment found so far is the A15 extended fulleride Cs_3C_{60}, discovered in 2008 (Ref. 84). It has also the highest transition temperature ever seen in a molecular material, 38 K at 7 kbar pressure; however, at ambient pressure it is an insulator, showing antiferromagnetic ordering below 50 K. The crystal structure stays cubic throughout the whole temperature and pressure range and the anions are rotationally ordered. Magnetic measurements indicate an S=1/2 moment localized on the fulleride anions.[85] The other polymorph of Cs_3C_{60}, with fcc structure, behaves similarly with a somewhat lower T_c of 35 K and a magnetic transition below 10 K,[86] which is less well characterized because of ferrorotational disorder and because the crystal structure does not permit full antiferromagnetic ordering. NMR measurements[87,88] prove both polymorphs metallic in the high-pressure phase above T_c.

A low-spin state in a symmetric environment can only occur if there is a symmetry-breaking mechanism other than the crystal field, and the molecular Jahn–Teller effect is the obvious candidate. As the splitting of vibrational bands mimics that of the electronic ones, infrared spectroscopy is an excellent indicator of molecular distortions[15,33] and can distinguish between the schemes shown in Fig. 3.

The infrared spectrum at ambient pressure is typical of an insulator at all temperatures, with a low background and Lorentzian lineshapes for the vibrational bands (Fig. 5). The Jahn–Teller effect in these materials turns out to be dynamic on a time scale comparable to that of the infrared measurement. The splitting of the infrared bands (Fig. 17) proves the symmetry lowering and shows a continuous temperature dependence which can be explained by the concept of temperature-dependent solid-state conformers applied for Jahn–Teller systems (two distorted conformers with their population changing on heating).[18]

Thus, Cs_3C_{60} proves the Mott transition and the Jahn–Teller effect to be the driving force behind the metal-insulator transitions in fulleride salts. Intense theoretical work towards the explanation of their superconductivity complements these experimental findings.[2]

6 Conclusions

In one of the earliest review papers on alkali fullerides,[7] Haddon stated: "Although the nature of the pairing mechanism in the A_3C_{60} superconductors remains to be established, the simplicity of the materials and the progress already made suggest that a definitive resolution of this question may be achieved more quickly than in the case of the high–T_c copper oxide superconductors." The bad news is that after twenty years, the race is still on; as in the cuprates, not only the superconducting state remains unexplained, but many normal-state properties as well. The good news, however, consists of the many new experimental facts and theoretical concepts that have emerged along the way and the hope that the two problems may finally

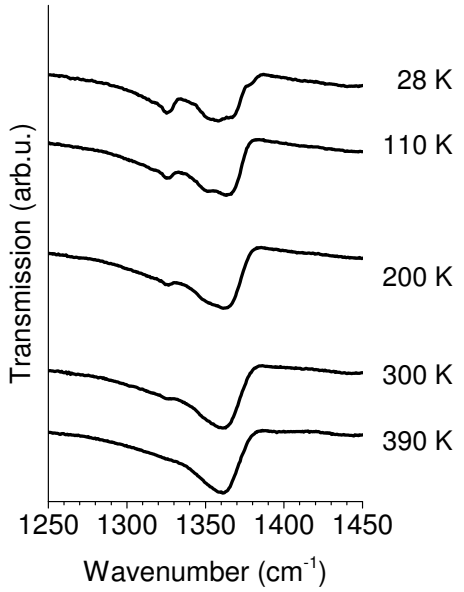

Fig. 17 Jahn–Teller splitting of the $T_{1u}(4)$ mode in A15 Cs_3C_{60}.[33]

converge into one solution.[89] One should not forget the fruitful dialogue that emerged between many disciplines from condensed matter theory and quantum chemistry to sophisticated physical methods and molecular spectroscopy to explore these beautiful structures full of surprises at every step.

7 Acknowledgements

The authors are grateful to R. C. Haddon, A. F. Hebard, Y. Iwasa, P. B. Littlewood, P. Matus, G. Oszlányi, S. Pekker, K. Prassides, M. J. Rosseinsky, P. Rudolf, D. B. Tanner and E. Tosatti for inspiration and enlightening discussions. This work was supported by the Hungarian National Research Fund (OTKA) through grant No. 105691.

References

1 L. Forró and L. Mihály, *Rep. Prog. Phys.*, 2001, **64**, 649–699.
2 M. Capone, M. Fabrizio, C. Castellani and E. Tosatti, *Rev. Mod. Phys.*, 2009, **81**, 943–958.
3 Y. Iwasa and T. Takenobu, *J. Phys.: Condens. Matter*, 2003, **15**, R495–R519.
4 A. F. Hebard, *Physics Today*, 1992, **45**, 26–32.
5 C. H. Pennington and V. A. Stenger, *Rev. Mod. Phys.*, 1996, **68**, 855–910.
6 R. C. Haddon, L. E. Brus and K. Ragavachari, *Chem. Phys. Lett.*, 1986, **125**, 459–464.
7 R. C. Haddon, *Acc. Chem. Res.*, 1992, **25**, 127–133.
8 S. Saito and A. Oshiyama, *Phys. Rev. Lett.*, 1991, **66**, 2637–2640.
9 S. C. Erwin and W. E. Pickett, *Science*, 1991, **254**, 842–845.
10 Y. Iwasa, K. Tanaka, T. Yasuda and T. Koda, *Phys. Rev. Lett.*, 1992, **69**, 2284–2287.
11 T. T. M. Palstra, R. C. Haddon, A. F. Hebard and J. Zaanen, *Phys. Rev. Lett.*, 1992, **68**, 1054–1057.
12 A. F. Hebard, T. T. M. Palstra, R. C. Haddon and R. M. Fleming, *Phys. Rev. B*, 1993, **48**, 9945–9948.
13 N. F. Mott, *Proc. Phys. Soc. London Ser. A*, 1949, **62**, 416–421.
14 N. F. Mott, *Metal-insulator transitions*, Taylor and Francis, London, 1990.
15 G. Klupp, K. Kamarás, N. M. Nemes, C. M. Brown and J. Leao, *Phys. Rev. B*, 2006, **73**, 085415–1–12.
16 C. A. Kuntscher, G. M. Bendele and P. W. Stephens, *Phys. Rev. B*, 1997, **55**, R3366–R3369.
17 C. C. Chancey and M. C. M. O'Brien, *The Jahn-Teller Effect in C_{60} and Other Icosahedral Complexes*, Princeton University Press, Princeton, 1997.
18 I. B. Bersuker, *The Jahn-Teller Effect*, Cambridge University Press, Cambridge, 2006.
19 Y. Tokura and N. Nagaosa, *Science*, 2000, **288**, 462–468.
20 S. Tomita, J. U. Andersen, E. Bonderup, P. Hvelplund, B. Liu, S. B. Nielsen, U. V. Pedersen, J. Rangama, K. Hansen and O. Echt, *Phys. Rev. Lett.*, 2005, **94**, 053002–1–4.
21 C. A. Reed and R. D. Bolskar, *Chem. Rev.*, 2000, **100**, 1075–1120.
22 P. Paul, Z. Xie, R. Bau, P. D. W. Boyd and C. A. Reed, *J. Am. Chem. Soc.*, 1994, **116**, 4145–4146.
23 P. Dahlke and M. J. Rosseinsky, *Chem. Mater.*, 2002, **14**, 1285–1291.
24 M. Fabrizio and E. Tosatti, *Phys. Rev. B*, 1997, **55**, 13465–13472.
25 M. Capone, M. Fabrizio, P. Giannozzi and E. Tosatti, *Phys. Rev. B*, 2000, **62**, 7619–7624.
26 G. Klupp and K. Kamarás, in *The Jahn-Teller effect: Fundamentals and Implications for Physics and Chemistry*, ed. H. Köppel, D. R. Yarkony and H. Barentzen, Springer, 2009, vol. 97, pp. 489–516.
27 M. Dressel and G. Grüner, *Electrodynamics of solids*, Cambridge University Press, Cambridge, 2002.
28 L. Degiorgi, E. Nicol, O. Klein, G. Grüner, P. Wachter, S.-M. Huang, J. Wiley and R. Kaner, *Phys. Rev. B*, 1994, **49**, 7012–7025.
29 Y. Iwasa and T. Kaneyasu, *Phys. Rev. B*, 1995, **51**, 3678–3685.
30 W. Krätschmer, K. Fostiropoulos and D. R. Huffman, *Chem. Phys. Lett.*, 1990, **170**, 167–170.
31 A. Pekker, F. Borondics, K. Kamarás, A. Rinzler and D. Tanner, *Phys. Stat. Sol. (b)*, 2006, **243**, 3485–3488.
32 G. Klupp, P. Matus, K. Kamarás, A. Y. Ganin, A. McLennan, M. J. Rosseinsky, Y. Takabayashi, M. T. McDonald and K. Prassides, *Nat. Commun.*, 2012, **3**, 912–1–6.
33 K. Kamarás, G. Klupp, P. Matus, A. Y. Ganin, A. McLennan, M. J. Rosseinsky, Y. Takabayashi, M. T. McDonald and K. Prassides, *J. Phys.: Conf. Ser.*, 2013, **428**, 012002–1–6.
34 U. Fano, *Phys. Rev.*, 1961, **124**, 1866–1878.
35 D. B. Tanner, C. S. Jacobsen, A. A. Bright and A. J. Heeger, *Phys. Rev. B*, 1977, **16**, 3283–3290.
36 (*a*) K. Kamarás, L. Forró and Y. Iwasa, *Phys. Rev. B*, 1997, **55**, 10999–11002; (*b*) K. Kamarás, L. Forró and Y. Iwasa, *Phys. Rev. B*, 1998, **57**, 5543.
37 V. C. Long, J. L. Musfeldt, K. Kamarás, G. B.Adams, J. B.Page, Y.Iwasa and W. E.Mayo, *Phys. Rev. B*, 2000, **61**, 13191–13201.
38 Z.-T. Zhu, J. L. Musfeldt, K. Kamarás, G. B. Adams, J. B. Page, V. A. Davydov, L. S. Kashevarova and A. V. Rakhmanina, *Phys. Rev. B*, 2002, **65**, 085413–1–9.
39 Z.-T. Zhu, J. L. Musfeldt, K. Kamarás, G. B. Adams, J. B. Page and V. A. Davydov, *Phys. Rev. B*, 2003, **67**, 045409–1–9.
40 T. Pichler, R. Winkler and H. Kuzmany, *Phys. Rev. B*, 1994, **49**, 15879–15889.
41 A. M. Rao, P. C. Eklund, J.-L. Hodeau, L. Marques and M. Nunez-Regueiro, *Phys. Rev. B*, 1997, **55**, 4766.

42 K. Kamarás, G. Klupp, D. B. Tanner, A. F. Hebard, N. M. Nemes and J. E. Fischer, *Phys. Rev. B*, 2002, **65**, 052103–1–4.

43 A. Auerbach, N. Manini and E. Tosatti, *Phys. Rev. B*, 1994, **49**, 12998–13007.

44 M. Martin, D. Koller and L. Mihaly, *Phys. Rev. B*, 1993, **47**, 14607–14610.

45 T. T. M. Palstra, A. F. Hebard, R. C. Haddon and P. B. Littlewood, *Phys. Rev. B*, 1994, **50**, 3462–3465.

46 P. Matus, G. Klupp, K. Kamarás, M. Roubelakis and K. Prassides, unpublished.

47 (*a*) T. Timusk and D. B. Tanner, in *Physical Properties of High-Temperature Superconductors I*, ed. D. M. Ginsberg, World Scientific, Singapore, 1989, pp. 339–407; (*b*) D. B. Tanner and T. Timusk, in *Physical Properties of High-Temperature Superconductors III*, ed. D. M. Ginsberg, World Scientific, Singapore, 1992, pp. 363–469.

48 T. Sasaki, I. Ito, N. Yoneyama, N. Kobayashi, N. Hanasaki, H. Tajima, T. Ito and Y. Iwasa, *Phys. Rev. B*, 2004, **69**, 064508–1–7.

49 M. Knupfer and J. Fink, *Phys. Rev. Lett.*, 1997, **79**, 2714–2717.

50 S. Pekker, L. Forró, L. Mihály and A. Jánossy, *Solid State Commun.*, 1994, **90**, 349–352.

51 H. Kuzmany, R. Winkler and T. Pichler, *J. Phys.: Condens. Matter*, 1995, **7**, 6601–6624.

52 K. Kamarás, L. Gránásy, D. B. Tanner and L. Forró, *Phys. Rev. B*, 1995, **52**, 11488–11491.

53 K. Kamarás, S. Pekker, L. Forró and D. B. Tanner, *Chem. Phys. Lett.*, 1998, **295**, 279–284.

54 K. Kamarás, D. B. Tanner and L. Forró, *Fullerene Sci. Tech.*, 1997, **5**, 465–478.

55 M. Martin, D. Koller, X. Du, P. W. Stephens and L. Mihaly, *Phys. Rev. B*, 1994, **49**, 10818–10821.

56 O. Chauvet, G. Oszlányi, L. Forro, P. W. Stephens, M. Tegze, G. Faigel and A. Jánossy, *Phys. Rev. Lett.*, 1994, **72**, 2721–2724.

57 F. Bommeli, L. Degiorgi, P. Wachter, Ö. Legeza, A. Jánossy, G. Oszlanyi, O. Chauvet and L. Forro, *Phys. Rev. B*, 1995, **51**, 14794–14797.

58 S. Pekker, G. Oszlányi and G. Faigel, *Chem. Phys. Lett.*, 1998, **282**, 435–441.

59 G. Oszlányi, G. Baumgartner, G. Faigel and L. Forró, *Phys. Rev. Lett.*, 1997, **78**, 4438–4441.

60 K. Prassides, K. Vavekis, K. Kordatos, K. Tanigaki, G. M. Bendele and P. W. Stephens, *J. Am. Chem. Soc.*, 1997, **119**, 834–835.

61 G. M. Bendele, P. W. Stephens, K. Prassides, K. Vavekis, K. Kordatos and K. Tanigaki, *Phys. Rev. Lett.*, 1998, **80**, 736–739.

62 V. Brouet, H. Alloul, S. Garaj and L. Forro, *Phys. Rev. B*, 2002, **66**, 155122–1–11.

63 Y. Kubozono, Y. Takabayashi, S. Fujiki, S. Kashino, T. Kambe, Y. Iwasa and S. Emura, *Phys. Rev. B*, 1999, **59**, 15062–15069.

64 G. Klupp, P. Matus, D. Quintavalle, L. Kiss, E. Kováts, N. Nemes, K. Kamarás, S. Pekker and A. Jánossy, *Phys. Rev. B*, 2006, **74**, 195402–1–7.

65 S. Margadonna, D. Pontiroli, M. Belli, T. Shiroka, M. Riccó and M. Brunelli, *J. Am. Chem. Soc.*, 2004, **126**, 15032–15033.

66 M. Riccó, T. Shiroka, M. Belli, D. Pontiroli, M. Pagliari, G. Ruani, D. Palles, S. Margadonna and M. Tomaselli, *Phys. Rev. B*, 2005, **72**, 155437–1–7.

67 M. Riccò, M. Belli, M. Mazzani, D. Pontiroli, D. Quintavalle, A. Jánossy and G. Csányi, *Phys. Rev. Lett.*, 2009, **102**, 145901–1–4.

68 R. Macovez, R. Savage, L. Venema, J. Schiessling, K. Kamarás and P. Rudolf, *J. Phys. Chem. C*, 2008, **112**, 2988–2996.

69 M. Riccó, M. Belli, D. Pontiroli, M. Mazzani, T. Shiroka, D. Arčon, A. Zorko, S. Margadonna and G. Ruani, *Phys. Rev. B*, 2007, **75**, 081401(R)–1–4.

70 D. Pontiroli, M. Aramini, M. Gaboardi, M. Mazzani, A. Gorreri, M. Riccò, I. Margiolaki and D. Sheptyakov, *Carbon*, 2013, **51**, 143–147.

71 C. M. Brown, S. Taga, B. Gogia, K. Kordatos, S. Margadonna, K. Prassides, Y. Iwasa, K. Tanigaki, A. N. Fitch and P. Pattison, *Phys. Rev. Lett.*, 1999, **83**, 2258–2261.

72 B. Gogia, K. Kordatos, H. Suematsu, K. Tanigaki and K. Prassides, *Phys. Rev. B*, 1998, **58**, 1077–1079.

73 D. Quintavalle, F. Borondics, G. Klupp, A. Baserga, F. Simon, A. Jánossy, K. Kamarás and S. Pekker, *Phys. Rev. B*, 2008, **77**, 155431–1–5.

74 P. Rudolf, R. Raval, P. Dumas and G. P. Williams, *Appl. Phys. A*, 2002, **75**, 147–153.

75 P. Dumas, M. Gruyters, P. Rudolf, Y. He, L.-M. Yu, G. Gensterblum, R. Caudano and Y. J. Chabal, *Surf. Sci.*, 1996, **368**, 330–336.

76 W. Erley and B. N. J. Persson, *Surf. Sci.*, 1989, **218**, 494–506.

77 K. Kamarás, K. Holczer and A. Jánossy, *Chem. Scripta*, 1981, **17**, 203–204.

78 O. Gunnarson, *Rev. Mod. Phys.*, 1997, **69**, 575–606.

79 P. Dahlke, M. S. Denning, P. F. Henry and M. J. Rosseinsky, *J. Am. Chem. Soc.*, 2000, **122**, 12352–12361.

80 M. J. Rosseinsky, D. W. Murphy, R. M. Fleming and O. Zhou, *Nature*, 1993, **364**, 425–427.

81 H. Kitano, R. Matsuo, K. Miwa, A. Maeda, T. Takenobu, Y. Iwasa and T. Mitani, *Phys. Rev. Lett.*, 2002, **88**, 096401–1–4.

82 K. Ishii, T. Watanuki, A. Fujiwara, H. Suematsu, Y. Iwasa, H. Shimoda, T. Mitani, H. Nakao, Y. Fujii, Y. Murakami and H. Kawada, *Phys. Rev. B*, 1999, **59**, 3956–3960.

83 N. Manini, G. E. Santoro, A. Dal Corso and E. Tosatti, *Phys. Rev. B*, 2002, **66**, 115107–1–7.

84 A. Y. Ganin, Y. Takabayashi, Y. Z. Khimyak, S. Margadonna, A. Tamai, M. J. Rosseinsky and K. Prassides, *Nat. Mater.*, 2008, **7**, 367–371.

85 Y. Takabayashi, A. Y. Ganin, P. Jeglič, D. Arčon, T. Takano, Y. Iwasa, Y. Ohishi, M. Takata, N. Takeshita, K. Prassides and M. J. Rosseinsky, *Science*, 2009, **323**, 1585–1590.

86 A. Y. Ganin, Y. Takabayashi, P. Jeglič, D. Arčon, A. Potočnik, P. J. Baker, Y. Ohishi, M. T. McDonald, M. D. Tzirakis, A. McLennan, G. R. Darling, M. Takata, M. J. Rosseinsky and K. Prassides, *Nature*, 2010, **466**, 221–227.

87 Y. Ihara, H. Alloul, P. Wzietek, D. Pontiroli, M. Mazzani and M. Riccò, *Phys. Rev. Lett.*, 2010, **104**, 256402–1–4.

88 Y. Ihara, H. Alloul, P. Wzietek, D. Pontiroli, M. Mazzani and M. Riccò, *Europhys. Lett.*, 2011, **94**, 37007.

89 E. Tosatti, *Science*, 2009, **323**, 1570–1571.